Supplementary material

Evaporating flow of liquid solutions in open rectangular microchannels

Panayiotis Kolliopoulos, Krystopher S. Jochem, Lorraine F. Francis, and Satish Kumar*

Department of Chemical Engineering and Materials Science, University of Minnesota, Minneapolis, MN 55455, USA

This document provides supplementary material on the empirical formulas used to describe the dependence of viscosity and surface tension on solute concentration and temperature, the method for calculating the rescaled cross-sectional-averaged dimensionless velocities $\bar{w}_i$, as well as the dimensionless parameter values used when comparing model predictions to experimental observations by Lade *et al.* (2018) in the primary article "Evaporating flow of liquid solutions in open rectangular microchannels".

S1 Constitutive equations for viscosity and surface tension

The constitutive equations for viscosity M and surface tension Σ depend on the liquid solution we choose to study. In this work, we use aqueous poly(vinyl alcohol) (PVA) solutions and compare model predictions to capillary-flow experiments conducted by Lade *et al.* (2018). An empirical model proposed by Patton (1964) is used to capture the dependence of viscosity on $\bar{T}$ and $\bar{c}$ through

$$\log M = \frac{\bar{c}}{k_a(\bar{T}) + \bar{c}k_b(\bar{T})}, \quad \text{where} \quad \begin{aligned} k_a(\bar{T}) &= 1.28 \times 10^{-5}(\hat{T}_V + \bar{T}\Delta\hat{T}) + 1.59 \times 10^{-2}, \\ k_b(\bar{T}) &= 3.83 \times 10^{-4}(\hat{T}_V + \bar{T}\Delta\hat{T}) - 2.47 \times 10^{-2}. \end{aligned} \tag{S1}$$

The $k_a(\bar{T})$ and $k_b(\bar{T})$ functions were reported by Lade *et al.* (2018) after fitting the empirical model to rheological data of PVA solutions for a range of temperatures and concentrations. In (S1), increasing the solute concentration can increase the viscosity by orders of magnitude, and increasing the temperature decreases the viscosity but does not change its order of magnitude. Similar models can be used to describe any solution or colloidal suspension where the shear viscosity is the dominant rheological parameter.

*kumar030@umn.edu

The effects of $\bar{T}$ and $\bar{c}$ on the surface tension are modeled using

$$\Sigma = 1 - Ma_c \bar{c}^{1/2} - Ma_T \bar{T}, \tag{S2}$$

where $Ma_c = \hat{\gamma}_c \epsilon / \hat{\mu}_0 \hat{U}$ is the solutal Marangoni number and $Ma_T = \hat{\gamma}_T \Delta \hat{T} \epsilon / \hat{\mu}_0 \hat{U}$ is the thermal Marangoni number, which are ratios of surface-tension-gradient forces to viscous forces, and $\hat{\gamma}_c$ and $\hat{\gamma}_T$ are experimentally obtained constants. We assume the temperature at the liquid-air interface does not deviate much from the vapor temperature, which allows us to write the surface tension as a linear function of $\bar{T}$ (Ajaev, 2005; Burelbach *et al.*, 1988; Craster *et al.*, 2009; Gramlich *et al.*, 2002). Many prior studies assume a dilute solution and use a linearized surface-tension dependence on the concentration (e.g., Lam & Benson (1970); Pham *et al.* (2017)); this would yield results that are qualitatively similar to those obtained using (S2). Comparison of the empirical models in (S1) and (S2) to the experimental results of Lade *et al.* (2018) is found in figure S1.

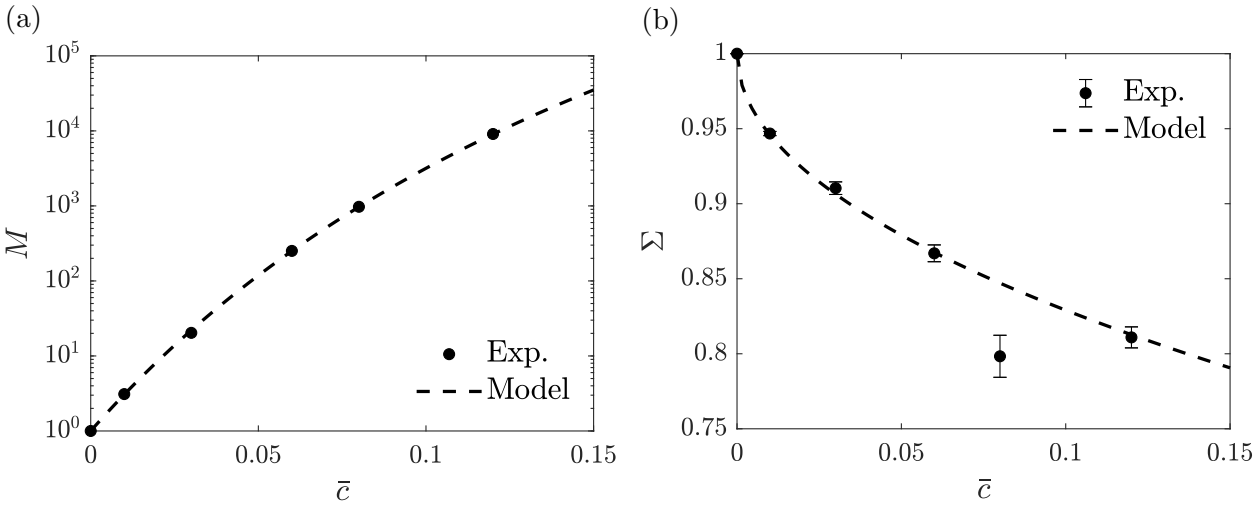

Figure S1: (a) Dimensionless viscosity M and (b) dimensionless surface tension Σ as a function of PVA concentration $\bar{c}$. Symbols represent experimental measurements by Lade *et al.* (2018) and dashed lines respresent model predictions using (S1) and (S2), respectively.

S2 Velocity Field

Here, we describe the method for calculating cross-sectional-averaged dimensionless velocities $\bar{U}_i^c(A)$ and $\bar{U}_i^g(A)$ seen in (2.29), with the subscript i being equal to D, R, T, or C for the meniscus-deformation, meniscus-recession, corner-transition, and corner-flow regimes,

respectively. The axial velocity w can be decomposed to two parts $w = w^c + w^g$, since (2.4) is linear in w, where w^c and w^g satisfy the following equations

$$p_z = M(w^c_{xx} + w^c_{yy}), \tag{S3a}$$

$$0 = w^g_{xx} + w^g_{yy}, \tag{S3b}$$

with boundary conditions

$$w^c = 0, \quad w^g = 0 \quad \text{at solid boundaries} \tag{S4a}$$

$$w^c_y - h_x w^c_x = 0, \quad M(w^g_y - h_x w^g_x) = \Sigma_z \quad \text{at free surface.} \tag{S4b}$$

Here, w^c is the contribution from the capillary-pressure gradient and w^g is the contribution from the Marangoni stresses.

S2.1 Meniscus-deformation and meniscus-recession regimes

To calculate $\bar{U}^c_i$ and $\bar{U}^g_i$ (where $i = D, R$) we rescale the velocities w^c and w^g as follows

$$w^c = -\frac{p_z}{M}\tilde{w}^c \quad \text{and} \quad w^g = \frac{\Sigma_z}{M}\tilde{w}^g. \tag{S5}$$

The rescaled velocities $\tilde{w}^c$ and $\tilde{w}^g$ then satisfy the following systems

$$\tilde{w}^c_{xx} + \tilde{w}^c_{yy} = -1, \quad \tilde{w}^c = 0 \quad \text{at solid boundaries,} \quad \tilde{w}^c_y - h_x \tilde{w}^c_x = 0 \quad \text{at free surface,} \tag{S6}$$

and

$$\tilde{w}^g_{xx} + \tilde{w}^g_{yy} = 0, \quad \tilde{w}^g = 0 \quad \text{at solid boundaries,} \quad \tilde{w}^g_y - h_x \tilde{w}^g_x = 1 \quad \text{at free surface,} \tag{S7}$$

where h is given in (2.6) for each regime. The cross-sectional-averaged dimensionless velocities $\bar{U}^c_i$ and $\bar{U}^g_i$ are defined as

$$\bar{U}^c_i = \frac{1}{A}\int_A \tilde{w}^c \, \mathrm{d}A \quad \text{and} \quad \bar{U}^g_i = \frac{1}{A}\int_A \tilde{w}^g \, \mathrm{d}A, \quad \text{for } i = D, R \tag{S8}$$

where A is given in (2.6). Note that the dependence of $\bar{U}^c_i(A)$ and $\bar{U}^g_i(A)$ on A is obtained by varying the contact angle $\theta \in [\pi/2, \theta_0]$ for $i = D$, and the liquid height on the side walls $a \in [1, W\lambda_c]$ for $i = R$ to create different cross sections characterized by h.

S2.2 Corner-transition and corner-flow regimes

To calculate $\bar{U}_i^c$ and $\bar{U}_i^g$ (where $i = T, C$) we rescale the velocities w^c and w^g and the coordinates as follows

$$x = a\tilde{x}, \quad y = a\tilde{y}, \quad h = a\tilde{h} \quad w^c = -a^2\frac{p_z}{M}\tilde{w}^c, \quad w^g = -a\frac{\Sigma_z}{M}\tilde{w}^g. \tag{S9}$$

The rescaled velocities $\tilde{w}^c$ and $\tilde{w}^g$ then satisfy the following systems

$$\tilde{w}^c_{\tilde{x}\tilde{x}} + \tilde{w}^c_{\tilde{y}\tilde{y}} = -1, \quad \tilde{w}^c = 0 \quad \text{at solid boundaries}, \quad \tilde{w}^c_{\tilde{y}} - \tilde{h}_{\tilde{x}}\tilde{w}^c_{\tilde{x}} = 0 \quad \text{at free surface}, \tag{S10}$$

and

$$\tilde{w}^g_{\tilde{x}\tilde{x}} + \tilde{w}^g_{\tilde{y}\tilde{y}} = 0, \quad \tilde{w}^g = 0 \quad \text{at solid boundaries}, \quad \tilde{w}^g_{\tilde{y}} - \tilde{h}_{\tilde{x}}\tilde{w}^g_{\tilde{x}} = 1 \quad \text{at free surface}, \tag{S11}$$

where $\tilde{h} = h/a$, and h is given in (2.6) for each regime. The cross-sectional-averaged dimensionless velocities $\bar{U}_i^c$ and $\bar{U}_i^g$ are defined as

$$\bar{U}_i^c = \frac{1}{\tilde{A}}\int_{\tilde{A}} \tilde{w}^c \, \mathrm{d}\tilde{A} \quad \text{and} \quad \bar{U}_i^g = \frac{1}{\tilde{A}}\int_{\tilde{A}} \tilde{w}^g \, \mathrm{d}\tilde{A}, \quad \text{for } i = T, C \tag{S12}$$

where $\tilde{A} = A/a^2$, and A is given in (2.6). Note that the dependence of $\bar{U}_T^c(A)$ and $\bar{U}_T^g(A)$ on A is obtained by varying the contact angle $\theta \in [\theta_T, \theta_0]$ to create different cross sections characterized by h. Because the rescaled cross-sectional area $\tilde{A} = B(\theta_0, \theta_0)/(\cos\theta_0 - \sin\theta_0)^2$ for the corner-flow regime, (S10) only needs to be solved once to obtain $\bar{U}_C^c(A)$ and $\bar{U}_C^g(A)$ for a given θ_0.

S3 Comparison to Experiments

The dimensionless parameter values used in figure 15 to compare model predictions to experimental observations by Lade *et al.* (2018) are shown in table S1.

Table S1: Parameter values used in figure 15.

λ	0.94	0.94	0.23	0.23
R_H	0.45	0.80	0.45	0.80
ϵ	1.6×10^{-3}	1.6×10^{-3}	1.6×10^{-3}	1.6×10^{-3}
λ_R	0.031	0.031	0.031	0.031
f_R	0.21	0.21	0.85	0.85
K	10.57	5.96	16.01	9.75
δ	1.58×10^{-5}	8.87×10^{-5}	1.58×10^{-5}	8.87×10^{-5}
Pe	4.03×10^{6}	4.03×10^{6}	4.03×10^{6}	4.03×10^{6}
E	0.323	0.059	0.323	0.059
Ma_T	1.81×10^{-2}	3.33×10^{-3}	1.81×10^{-2}	3.33×10^{-3}
Ma_c	0.54	0.54	0.54	0.54
α_E	5.0×10^{-3}	5.4×10^{-3}	3.3×10^{-3}	3.3×10^{-3}
C_0	0.03	0.03	0.03	0.03
θ_0	24.9	24.9	24.9	24.9

S4 Thermal accommodation coefficient α_E

Figure S2a demonstrates the effect of α_E on the meniscus and finger tip evolution. Increasing α_E increases the evaporation rate, leading to longer flow distances. As alluded to in §4.2, the maximum meniscus and finger tip flow distances scale as $\sim \hat{j}^{-1/2}$. Since, $\hat{j} \sim \alpha_E$ from (2.9), it follows that the maximum meniscus and finger tip flow distances scale as $\sim \alpha_E^{-1/2}$, which is confirmed in figure S2b.

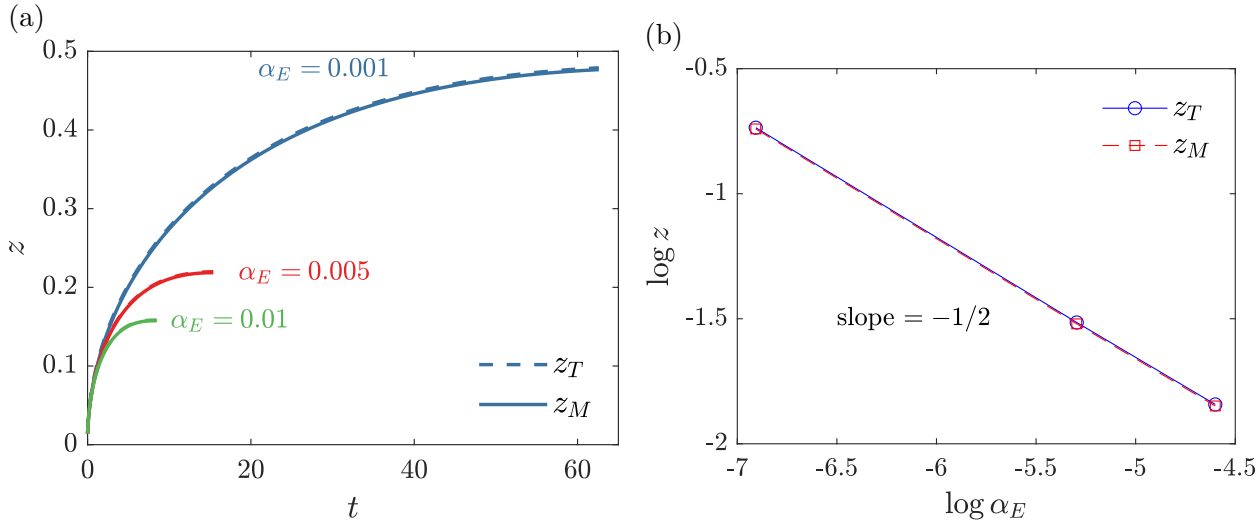

Figure S2: Effect of accomodation coefficient α_E on (a) evolution of meniscus position z_M and finger tip position z_T, and (b) maximum meniscus and finger tip position. Unless denoted otherwise, the parameter values are $\theta_0 = 24.9°$ ($\lambda_c = 0.32$), $\epsilon = 1.6 \times 10^{-3}$, $f_R = 0.21$, $R_H = 0.45$, $E = 0.323$, $Ma_c = 0.54$, $Ma_T = 1.81 \times 10^{-2}$, $K = 52.84$ ($\alpha_E = 10^{-3}$), $K = 10.57$ ($\alpha_E = 5 \times 10^{-3}$), $K = 5.28$ ($\alpha_E = 10^{-2}$), $\delta = 1.58 \times 10^{-5}$, $\alpha_E = 5 \times 10^{-3}$, and $Pe = 4.03 \times 10^6$.

References

Ajaev, V. S. 2005 Spreading of thin volatile liquid droplets on uniformly heated surfaces. *J. Fluid Mech.* **528**, 279–296.

Burelbach, J. P., Bankoff, S. G. & Davis, S. H. 1988 Nonlinear Stability of Evaporating Condensing Liquid-Films. *J. Fluid Mech.* **195**, 463–494.

Craster, R. V., Matar, O.K. & Sefiane, K. 2009 Pinning, Retraction, and Terracing of Evaporating Droplets Containing Nanoparticles. *Langmuir* **25** (6), 3601–3609.

Gramlich, C. M., Kalliadasis, S., Homsy, G. M. & Messer, C. 2002 Optimal leveling of flow over one-dimensional topography by Marangoni stresses. *Phys. Fluids* **14** (6), 1841–1850.

Lade, R. K. Jr., Jochem, K. S., Macosko, C. W. & Francis, L. F. 2018 Capillary Coatings: Flow and Drying Dynamics in Open Microchannels. *Langmuir* **34** (26), 7624–7639.

Lam, V. T. & Benson, G. C. 1970 Surface tensions of binary liquid systems. I. Mixtures of nonelectrolytes. *Can. J. Chem.* **48** (24), 3773–3781.

Patton, T. C. 1964 *Paint Flow and Pigment Dispersion*, 2nd edn. New York: John Wiley & Sons.

Pham, T., Cheng, X. & Kumar, S. 2017 Drying of Multicomponent Thin Films on Substrates with Topography. *J. Polym. Sci. Pol. Phys.* **55**, 1681–1691.